Effect of Molecular Properties of Block Copolymers and Nanoparticles on the Morphology of Self-Assembled Bulk Nanocomposites

Chieh-Tsung Lo,[†] Byeongdu Lee,[†] Vilas G. Pol,[||] Nancy L. Dietz Rago,[‡] Soenke Seifert,[†] Randall E. Winans,[†,§] and P. Thiyagarajan*[,||]

X-ray Science Division, Chemical Engineering Division, Chemistry Division, and Intense Pulsed Neutron Source, Argonne National Laboratory, 9700 S. Cass Avenue, Argonne, Illinois 60439

Received April 9, 2007; Revised Manuscript Received August 2, 2007

ABSTRACT: Self-assembly of thiol-terminated polystyrene-tethered Au nanoparticles in microphase-separated diblock copolymers composed of poly(styrene-*b*-2vinylpyridine) (PS−PVP) as a function of particle concentration and composition of block copolymers was investigated using anomalous small-angle X-ray scattering (ASAXS) and transmission electron microscopy (TEM). Results reveal that the self-assembly of nanoparticles in the PS domain causes swelling and increases the interfacial curvature that, in turn, induces order−order transitions. At intermediate loading, the presence of nanoparticles amplifies the local compositional fluctuations, hence the roughness at the PS and PVP interface, which creates conditions to induce disorder in the polymer morphology. The system thus undergoes an order−disorder transition. At high particle loading, packing constraints prevent all particles from assembling in the PS domain, and the excess nanoparticles undergo macrophase separation. The present systematic study augments experimental data to the scarce literature on the phase behavior of bulk nanocomposites. We present a generalized phase map for the bulk composites as a function of effective volume fraction of PS (F_{PS}) for a given nanoparticle size. We believe that the results from this study will enable comparison of the phase maps from various studies and will serve to validate the simulation studies of inorganic particle/block copolymer composites.

Introduction

Intense worldwide research is ongoing to develop polymer-based nanocomposites to exploit their unique properties. To achieve a higher level of control of the dispersion state of the inorganic particles and the morphology of the polymer matrix in the composites, new synthetic routes are being developed to manipulate both the inorganic fillers and the polymers at the nanoscale. Recently, it has been suggested that block copolymers with their rich diversity of morphologies arising from their microphase separation property can provide an effective means to control the particle location and dispersion. This technique, based on the self-assembly of nanoparticles into one microdomain of the block copolymers, is versatile to prepare nanocomposites with different polymer morphologies with particles organized in a variety of patterns. Such spatially regular composites will have high impact in nanotechnology, exploiting their unique magnetic,[1] optical,[2−5] electrical,[6,7] and mechanical[8] properties. Materials with better 2D and 3D ordering of nanoparticles in ordered polymer-based nanocomposites can serve as candidates for future advanced catalysts, selective membranes, and magnetic and photonic band gap materials.[9−15]

A few approaches have been proposed for the incorporation of nanoparticles selectively into the preferred domain of block copolymers to create 2D and 3D spatial distribution of nanoparticles in polymer matrices.[16−26] Since the properties of the nanocomposites strongly depend on the nature of dispersion as well as ordering of particles in the polymer matrix, tailoring nanoparticles into arrays in an ordered polymer phase will provide exciting new possibilities on the materials front. Thus, a detailed understanding of the effects of the molecular properties of block copolymers and nanoparticles on the self-assembled structures of the nanocomposites is essential to develop strategies to fabricate novel composites with unique structural and functional properties.

To gain a better insight into the thermodynamic aspects of organizing nanoparticles in ordered microphase-separated domains, several theoretical and experimental studies have been carried out. Using a Monte Carlo simulation and scaling theory, Huh et al.[27] investigated the phase behavior of polymer nanocomposites as a function of particle size and volume fraction. These studies showed that equilibrium morphologies form under the excluded volume constraints for the polymer chains and nanoparticles in the strong segregation limit of the copolymers and the addition of particles in the preferred domain causes phase transformations. However, if the particle sizes are comparable to the radius of gyration of the minority block, a macrophase separation of particles occurs that coexist with the fairly disordered block copolymer morphology. Another theoretical model that combines a self-consistent field theory (SCFT) for polymers and a density functional theory (DFT) for particles[4,14,28−33] was used to probe the relative entropic contributions of both the copolymer and particle and the enthalpic contribution between copolymer and particles on the microstructure of the composites. From the density profiles, it was shown that larger particles organize at the center of the preferred domain to reduce the overall free energy, while the smaller particles concentrate at the polymer interface to gain maximum translational entropy.[14,28−31] In addition to the thermodynamic properties of the particles and the polymer, the structural order in the composites would also strongly depend

* To whom all correspondence should be addressed. E-mail: thiyaga@anl.gov.
[†] X-ray Science Division, Argonne National Laboratory.
[‡] Chemical Engineering Division, Argonne National Laboratory.
[§] Chemistry Division, Argonne National Laboratory.
[||] Intense Pulsed Neutron Source, Argonne National Laboratory.

10.1021/ma070835v CCC: $37.00
Published on Web 10/10/2007

on the particle size.[30] Investigations by Chervanyov and Balazs[34] showed that smaller particles cause a greater shift in the order−disorder transition temperature (ODT) than the larger ones. Detailed phase diagrams of block copolymer/nanoparticle composites as a function of particle size and the relative molecular interaction between particles and diblock copolymers were generated using discontinuous molecular dynamics simulation.[15] Recently, by using mean field SCFT calculations Reisler and Fredrickson[35] investigated the phase behavior of a blend of polymer-tethered nanoparticles and diblock copolymer and showed the pronounced effect of overall size of the particles including the shell on the region of microphase separation and ways to increase the loading of the nanoparticles in an ordered phase without macrophase separation by tuning the length and the number of tethered polymer chains in the shell. Experimental data are required to validate the results from the above theoretical studies on the phase behavior of the diblock copolymer/inorganic nanoparticle composites.

On the experimental front, a few studies have been published recently on ways to control the location of nanoparticles in the polymer matrix by tailoring their surfaces with different ligands.[5,19,21,26,36] We have studied the phase behavior of diblock copolymer/nanoparticle complex in a selective solvent.[37,38] Our studies show that mixing the solvent with the composites provides an additional degree of freedom to manipulate the microstructure of the composites. Favorable interaction between the ligand and one segment of the block copolymer enables sequestering of the nanoparticles in the preferred domain constituted by that segment. Size-selective organization of particles has been validated by Bockstaller et al.[23] A significant size difference between the two inorganic nanoparticles in their study revealed that the entropy is the driving force for the large particles to segregate in the favorable domain, while small particles to remain at the interface and this is consistent with the theoretical predictions.[14,28−31] However, if the nanoparticle size is comparable to the lamellar period of the block copolymers, local deformation will occur. In addition, distortion of the copolymer structure will occur at higher nanoparticle loading.[39] Kramer's group have investigated the effects of areal density of homopolymers on the nanoparticles on their location in diblock copolymer composites[40] and nanoparticle induced phase transitions in bulk diblock/inorganic particle composites.[41] Their studies show that nanoparticles with an areal density of tethered polymer less than 1.3 chains/nm^2 segregate at the block copolymer interface and those with higher coverage locate within the preferred domain. Furthermore, the variation in the solvent evaporation along the depth direction of the film of 100 μm thickness causes variation in the nanoparticle loading and hence the polymer morphology varies as a function of depth from the air/polymer interface. Jain et al.[42] studied the order−disorder transition of nanocomposites as a function of filler dimensionality. They found that, in addition to the energetic and entropic effects upon the addition of nanoparticles, the geometric effect also plays an important role on the morphology of the composites. For instance, it has been shown that the depression of ODT is not a simple function of dimensionality, and in fact, the rodlike fillers induce the largest depression in ODT.

Yeh et al.[43−45] studied the selectively dispersed CdS quantum dots in block copolymers. Morphological transformations have been observed with the introduction of nanoparticles from hexagonally packed cylinders (C) to lamellar structure (L) and from C to body centered-cubic packed spheres or simple-cubic spheres. Similar phase transformations from C to L[46] and from L to C[36] have been found in the Au nanoparticles/block copolymer system. Although these initial studies have demonstrated the effectiveness of leveraging the rich phase behavior of the block copolymer in ordering the nanoparticles within polymer matrices, systematic studies are scarce in the literature on the effects of molecular properties of nanoparticles as well as block copolymers on the morphology of nanocomposites. Fundamental understanding of the morphology as a function of properties of nanoparticles and block copolymers is essential for fabrication of highly ordered nanocomposites with hierarchical structures.

Table 1. Characteristics of PS−PVP Diblock Copolymers[a]

polymer	N_{PS}	N_{PVP}	f_{PS}	PDI
PS−PVP(24)	133	448	0.24	1.11
PS−PVP(57)	510	417	0.57	1.04
PS−PVP(65)	501	295	0.65	1.05
PS−PVP(68)	452	229	0.68	1.07
PS−PVP(87)	513	84	0.87	1.03

[a] Here N_{PS} and N_{PVP} are the degrees of polymerization of PS and PVP, respectively, f_{PS} is the volume fraction of PS in PS−PVP, and PDI is the polydispersity index.

In the present study we systematically investigated the effects of the molecular properties of the block copolymers (e.g., composition), particle loading and homopolymer content on the phase behavior of block copolymer/nanoparticle composites. The thiol-terminated polystyrene (PSSH) tethering of nanoparticles protects them from self-aggregation in the polymer phase. The nanoparticles were mixed with block copolymer solutions to form polymer nanocomposites. We considered composites of poly(styrene-*b*-2vinylpyridine) (PS−PVP) and Au nanoparticles. The structural characteristics of the nanocomposites were determined by anomalous small-angle X-ray scattering (ASAXS) and transmission electron microscopy (TEM). We present a generalized experimental phase map on polymer/inorganic nanocomposites as a function of effective volume fraction of PS in the diblock copolymer (F_{PS}) that will enable comparison with the phase maps from both simulation and experimental studies. Given that the literature is scarce with the experimental data on the phase behavior of diblock copolymer-based nanocomposites we believe that this paper will be valuable to the polymer and nanoscience communities.

Experimental Section

Sample Preparation. We followed the procedure in Yee et al.[47] to synthesize the PS tethered Au nanoparticles. An equimolar volume of hydrogen tetrachloroaurate(III) trihydrate ($HAuCl_4 \cdot 3H_2O$, Aldrich Chemical Co., Inc.) and thiol-terminated PS (M_n = 1500 g/mol, PDI = 1.10, Polymer Source, Inc.) were mixed in THF (≥99.9%, Aldrich Chemical Co., Inc.). After 30 min, a reducing agent of 1 M lithium triethylborohydride in THF (Superhydride, Aldrich Chemical Co., Inc.) was added dropwise in the mixture to produce Au nanoparticles. As prepared Au nanoparticles were stored at ambient condition for 1 day to ensure that the reaction is complete. Further purification of nanoparticles involved methanol to remove the residual ions and thiol groups. Agglomerates of nanoparticles that formed due to solubility issues were collected by centrifugation and the samples were dried at room temperature (weight ratio of Au to polymer ~0.2).

To prepare nanocomposites, a 2% (w/v) polymer solution comprising Au nanoparticles and PS−PVP block copolymers with different compositions of diblocks (Polymer Source, Inc) was dissolved in THF. Table 1 provides the molecular properties of these copolymers. Upon mixing, the PS tethered nanoparticles self-assemble in the PS domains of the PS−PVP. The solutions were cast on mica and epoxy resin to make bulk composites. After 1 day of drying at ambient condition, the films were annealed at 150

°C for 3 days. In the Results and Discussion section, we will address that these annealing conditions are adequate for the composites to reach conditions close to thermodynamic equilibrium as well as to maintain the stability of the dispersion of Au particles in them.

Small-Angle X-ray Scattering (SAXS). SAXS experiments were performed at Sector 12ID-C at Advanced Photon Source in Argonne National Laboratory to characterize the nanostructural morphology of PS−PVP/Au composites. Samples on mica were measured at room temperature with a sample to detector distance of ∼2 m. The data were corrected for incident flux, absorption, detector sensitivity variation, and dark current.

In the SAXS experiments, signals from the scattering of nanoparticles dominate that of the block copolymers and this makes it difficult to determine the morphology of the block copolymers. To delineate the partial scattering signal from the polymer phase of the composite we used ASAXS wherein multiple measurements were made using X-rays with different incident energies (E) near and below the L_3 edge of Au, 11.919 keV and the data were analyzed using the procedure in Lee et al.[48] In ASAXS, the scattering signal from the Au particles is strongly dependent on the X-ray energy while that from the polymer is energy independent. The scattering data measured at different energies were normalized at the high Q ($4\pi(\sin\theta)/\lambda$ where 2θ is the scattering angle and λ is the wavelength of X-rays) region that is mainly contributed by the nanoparticles.

Transmission Electron Microscopy (TEM). Bulk nanocomposites embedded in epoxy resin were sectioned to ∼80 nm with an Ultracut S microtome (Reichert, Leica, MI). To distinguish between the PS and PVP domains, specimens were stained by iodine vapor for 24 h. Iodine adsorbs to PVP that reveals as dark regions in TEM. A JEOL 2000 FX II transmission electron microscope operated at 200 kV was used to obtain images on the morphology of composites.

Results and Discussion

Au Nanoparticles. Figure 1a shows the SAXS data of the purified PS-tethered Au nanoparticles dispersed in THF. The data were fitted using the form factor of a spherical shell model[49] yielding a mean core radius of 10.8 Å corresponding to the Au and a polymer shell thickness of 7.3 Å. The root-mean squared spread of the core radius from the Shultz distribution is 6.7 Å. The mean overall diameter of PS-tethered Au nanoparticles is ∼36.2 Å. We also derived the size of the Au core of the Au nanoparticles in the bulk composites using the partial scattering function of Au moiety derived from the ASAXS of the composites that yielded a mean radius of 1 nm and a similar rms spread.[48] TEM of the composite in Figure 1b confirmed the SAXS result that the Au nanoparticles in the polymer phase are unaggregated as in solution.

Phase Behavior of PS−PVP/Au Nanocomposites. To illustrate and establish that the annealing temperature of 150 °C and 3 days time are optimal for the composites to reach conditions close to thermodynamic equilibrium and that the bare Au particles free of alkanethiol attached PS are well dispersed in the polymer matrix, we carried out SAXS experiments on three samples, a neat PS−PVP $f_{PS} = 0.57$ (f_{PS} is the volume fraction of PS in PS−PVP) and the same polymer with $\phi_{Au} =$ 17.9%, and that with $\phi_{Au} = 27.2\%$ (ϕ_{Au} is the volume fraction of Au nanoparticles in PS−PVP/Au composite, defined as $\phi_{Au} = V_{Au}/(V_{PS-PVP} + V_{Au})$, where V_{PS-PVP} and V_{Au} are the volumes of PS−PVP and PS-tethered Au nanoparticles, respectively). We used one set of the above-mentioned samples as control and annealed them at 150 °C for 3 days. An identical set of samples were annealed first at 150 °C for 3 days, followed by annealing at 180 °C for 1 day and back at 150 °C for 1 day. We believe that the additional annealing at higher temperature will increase the kinetics of relaxation of the polymers and enable the composites to reach conditions close to thermodynamic equilibrium.

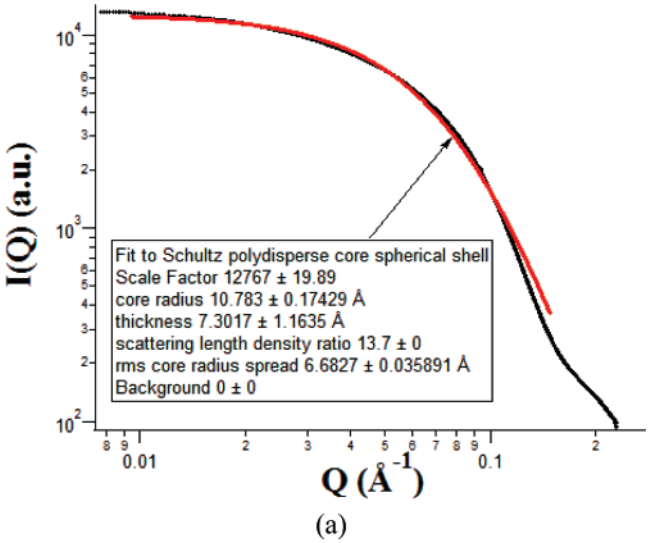

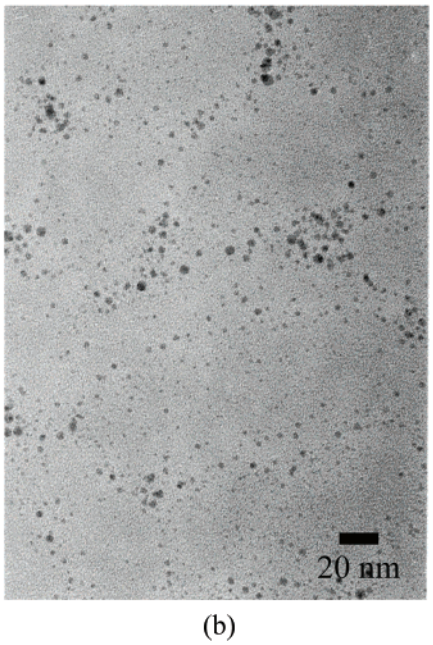

Figure 1. (a) SAXS data of PS-tethered Au nanoparticles in solution. The pattern was fitted by using the Schultz polydisperse core and spherical shell model. (b) TEM image of Au nanoparticles in the PS−PVP nanocomposite.

Figure 2a compares the SAXS data of the neat PS−PVP sample annealed at 150 °C for 3 days and that subjected to additional annealing at higher temperature. As expected, both samples exhibit over 6 orders of diffraction peaks corresponding to a highly ordered lamellar phase. In Figure 2b, we show SAXS data for the PS−PVP sample with $\phi_{Au} = 17.9\%$. It is clear from Figure 2b that these samples also exhibit a lamellar order, but we can see only three diffraction peaks that appear to be slightly broadened, implying the decrease in the ordering of the polymer phase. Another reason for the higher order peaks being invisible in the SAXS data might be due to the masking by the strong scattering signal from the Au particles in the high Q region. Since thiol bonds attached to Au nanoparticles are expected to break down during the above annealing temperatures for extended period it is of interest to learn about whether the bare Au particles aggregate during the anneal. Samples annealed at both conditions have similar scattering at $Q > 0.04$ Å^{-1} where

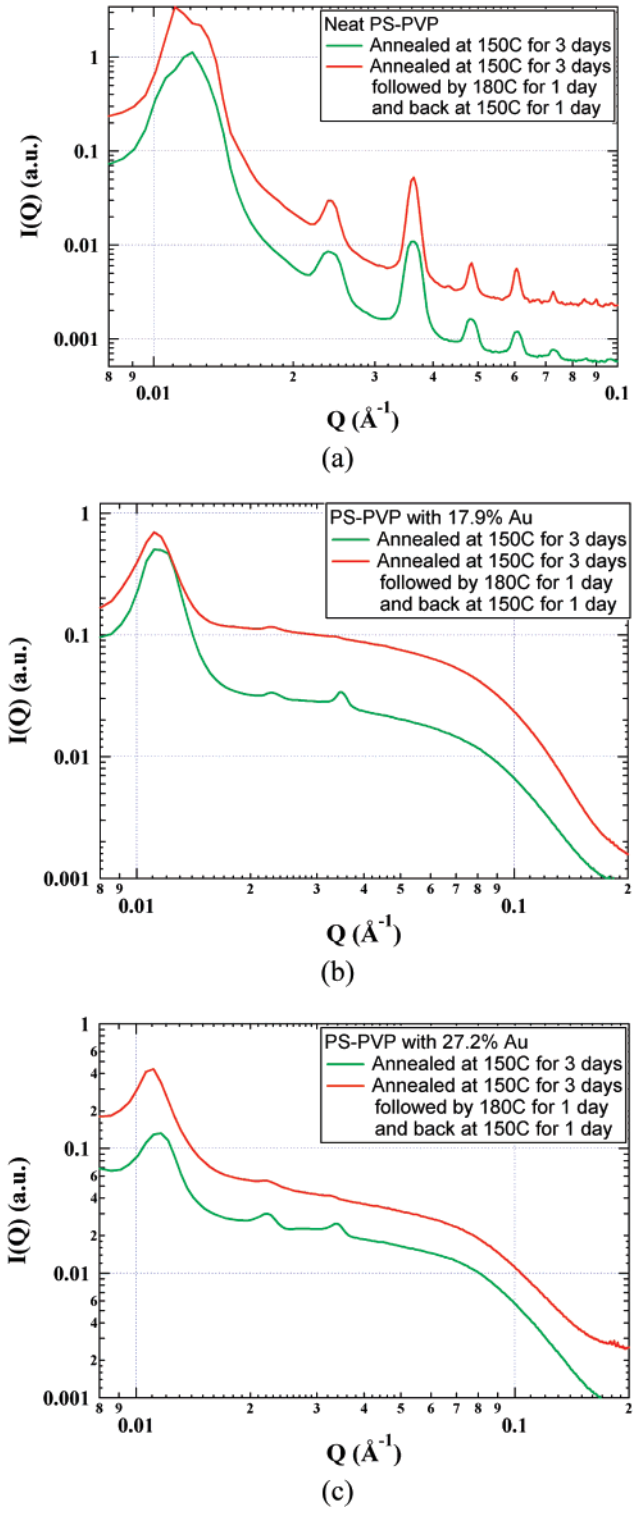

Figure 2. (a) Comparison of the SAXS data of PS−PVP ($f_{PS} = 0.57$) samples at two annealing conditions: (1) at 150 °C for 3 days and (2) at 150 °C for 3 days, followed by further annealing at 180 °C for 1 day and back at 150 °C for 1 day. Both samples show the expected high degree of lamellar ordering. (b) SAXS data of PS−PVP/Au nanocomposites ($f_{PS} = 0.57$, $\phi_{Au} = 17.9\%$) for the above annealing conditions. Both exhibit lamellar ordering and the Au nanoparticles are nicely dispersed as in solution (see the SAXS data in Figure 1). (c) SAXS data of PS−PVP/Au nanocomposites ($f_{PS} = 0.57$, $\phi_{Au} = 27.2\%$) for the above annealing conditions. These also exhibit lamellar ordering and the Au nanoparticles are nicely dispersed. The patterns are shifted to increase the clarity.

the SAXS signal from the Au particles dominates. Comparison of SAXS data in Figure 2b and Figure 1 clearly shows that the

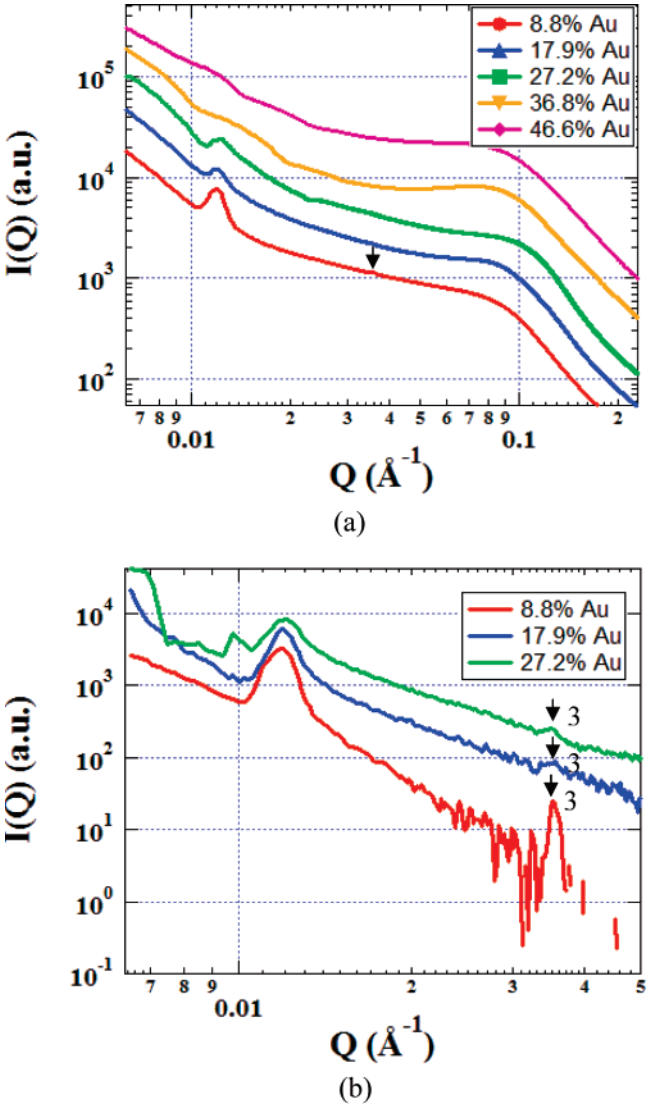

Figure 3. (a) SAXS data of PS−PVP/Au nanocomposites ($f_{PS} = 0.57$) using X-rays with $E = 11.919$ keV. (b) patterns after the subtraction of nanoparticle scatterings. (Scattering patterns have been shifted to increase clarity, and the arrows and numbers in the plots show the ratio of the peak positions to the value of the first-order peak.)

Au particles in the polymer phase remain well dispersed as in solution. Similar features are seen in Figure 2c that shows the SAXS data for the PS−PVP sample with $\phi_{Au} = 27.2\%$. In this case also both samples annealed at different conditions exhibit similar ordering in the polymer phase and well dispersed Au particles. On the basis of these results we conclude that the annealing time of 3 days at 150 °C seems adequate for the PS−PVP/Au nanocomposites to attain conditions close to thermodynamic equilibrium.

Figure 3a shows the SAXS patterns of the nanocomposites with $f_{PS} = 0.57$ (f_{PS} is the volume fraction of PS in PS−PVP) measured using X-rays with $E = 11.919$ keV. Distinct peaks in the low Q region corresponding to the copolymer phase are observed only for the composites with $\phi_{Au} \leq 27.2\%$. However, since higher order peaks are not visible in the data due to the dominant SAXS signal from Au particles, partial scattering functions of the block copolymer phase were deconvoluted from the ASAXS data measured at different energies below the L_3 edge of Au using the method in Lee et al.[48] The partial scattering functions for the composites with $\phi_{Au} \leq 27.2\%$ exhibit higher order peaks as shown in Figure 3b. The ratio of the higher order peaks to the first-order peak (Q/Q^*, where Q^* is the position

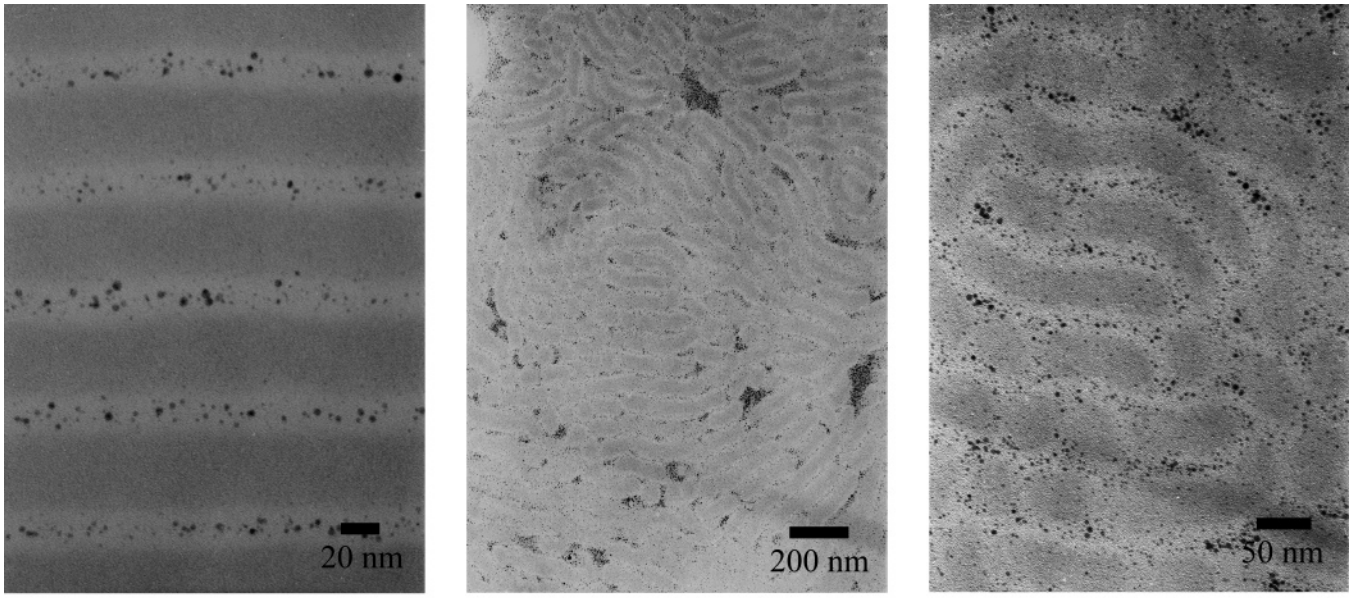

Figure 4. TEM images of PS−PVP/Au nanocomposites ($f_{PS} = 0.57$). Key: (a) $\phi_{Au} = 13.3\%$; (b) $\phi_{Au} = 27.2\%$ at 4000×; (c) $\phi_{Au} = 27.2\%$ at 150000×.

of the first-order peak) is 1:3. This suggests that the system has a lamellar structure and the absence of the second-order peak may presumably be due to about 1:1 thickness ratio of the block copolymer lamellae at lower composition of Au and the destructive interference between the weak structure factor and the form factor minima of the core−shell type polymer phase. At higher particle loading, the system becomes disordered, based on the disappearance of diffraction peaks, but the minima are still visible in Figure 3b, suggesting the presence of core−shell type lamellar phase containing Au. To complement these results we used TEM to determine the structural features of these nanocomposites. At $\phi_{Au} = 13.3\%$ (Figure 4a), nanoparticles are randomly distributed within the PS domains in a lamellar phase. At $\phi_{Au} = 27.2\%$ (Figure 4b), the available volume in the PS domains presumably saturates, and macrophase-separated regions of nanoparticles can be seen along with distorted lamellar regions. This behavior is consistent with the Monte Carlo simulation that particles segregate from diblock copolymers at high particle loading.[27] In the presence of nanoparticles in the PS domain, the PS chains surrounding the particles have to alter their conformation to accommodate the nanoparticles that costs additional energy. The PS chains normal to the interface have to stretch to release the energy, while the PVP chains normal to the interface will contract. Thus, the position of the PS−PVP interface strongly depends on the balance between the stretching of the PS chains and contracting PVP chains. This behavior induces local fluctuations and the composite forms distorted lamellar structures[46] as in Figure 4c.

Figure 5 shows TEM images of PS−PVP/Au with nanoparticles in the minor domain of the block copolymer ($f_{PS} < 0.5$). Here again, the addition of nanoparticles causes similar changes in polymer morphology. At $\phi_{Au} = 9.0\%$ (Figure 5a), the composite exhibits hexagonally packed cylindrical structure with nanoparticles located in the middle of the PS domain. At $\phi_{Au} = 27.7\%$ (Figure 5b), local fluctuations at the PS−PVP interface cause the formation of distorted cylinders. The SAXS patterns in Figure 6 for PS−PVP/Au composites with $\phi_{Au} \leq 27.7\%$ exhibit peaks with Q/Q^* of $1:\sqrt{3}:2:\sqrt{7}$, indicating the presence of hexagonally packed cylinders. The system becomes disordered at $\phi_{Au} = 37.4\%$. Interestingly, for composites with nanoparticles sequestered in the minor domain, the peak intensities are fairly stronger and conventional SAXS data are adequate to characterize the polymer morphology in the composites. We surmise that this is due to the fact that when nanoparticles are confined in the minor domain, their concentration when compared to the volume fraction of the polymer phase is relatively high and by virtue of their continuous dispersion within the domain they enhance the contrast between the particle rich PS and neat PVP domains and hence the structure factor. In contrast, when the nanoparticles disperse in the major domain, due to lower effective concentration and lack of connectivity of nanoparticles, they do not contribute constructively to the structure factor of the polymer phase.

From the TEM images of PS−PVP/Au with nanoparticles in either major or minor domains of the block copolymers, the resulting morphology with the addition of nanoparticles can be described using a model shown in Figure 7. At low particle loading, the nanoparticles are well organized in the preferred domain of the block copolymer (Figure 7a). As particle loading increases, the local concentration gradient of nanoparticles increases the interfacial roughness between two domains, inducing distortion in the morphology (Figure 7b). Above a threshold volume fraction of nanoparticles, the excess particles cannot assemble in the preferred domain, and the system undergoes a macrophase separation of particles coexisting with an ordered polymer/nanoparticle phase (Figure 7c).

On the basis of the SAXS and TEM results, a phase diagram for the nanocomposites as a function of f_{PS} and ϕ_{Au} has been generated as in Figure 8a. The results reveal that nanoparticles can be incorporated in lamellar and cylinder phases with nanoparticles in the major and minor domains of the block copolymers. Most of the nanocomposites maintain the morphology of neat block copolymers in the presence of nanoparticles up to a particle loading of $\phi_{Au} \sim 30\%$. Above that loading an order−disorder transition occurs, reminiscent of the behavior of block copolymers in a solvent. When the block copolymer is dispersed in a solvent, the solvent dilutes the ordered microdomains, leading to a reduction in the degree of segregation.[50−53] The addition of nanoparticles also weakens the degree of segregation and causes a vertical shift in the phase

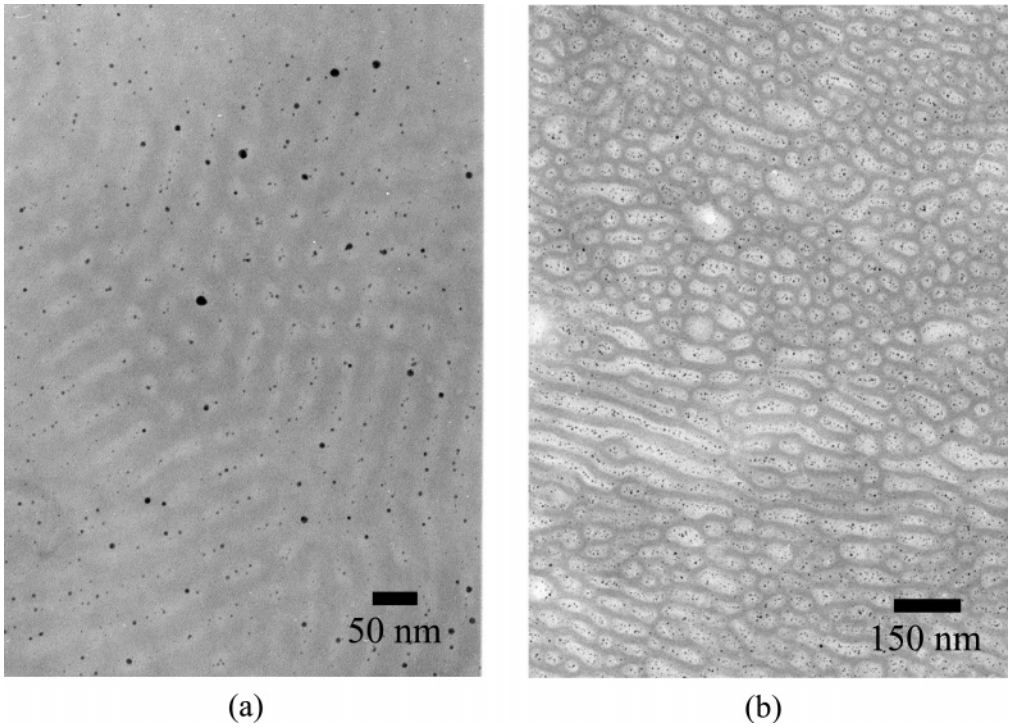

Figure 5. TEM images of PS−PVP/Au nanocomposites ($f_{PS} = 0.24$). Key: (a) $\phi_{Au} = 9.0\%$; (b) $\phi_{Au} = 27.7\%$.

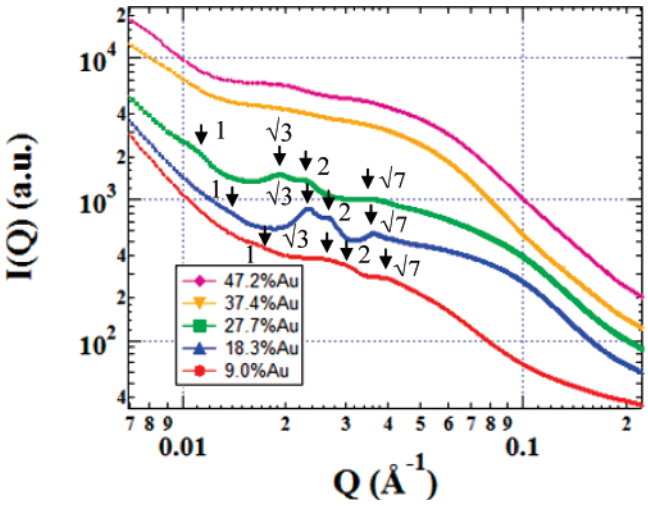

Figure 6. SAXS data of PS−PVP/Au nanocomposites ($f_{PS} = 0.24$) using X-rays with $E = 11.919$ keV. (Scattering patterns have been shifted to increase clarity, and the arrows and numbers in the plots show the ratio of the peak positions to the value of the first-order peak.)

map. It should be noted that this phenomenon is different from the effect of the addition of similar concentration of homopolymers in the preferred domain because the homopolymers can only swell the preferred domain and hence not expected to modify the degree of segregation.[54] Also, the addition of homopolymers can ease the excess interfacial energy and compensate for the deformation caused by the nanoparticles.[55] To confirm this effect, we added PSSH to PS−PVP(68) and the morphology of the composites was investigated using SAXS and the results are shown in Figure 9. At $\phi_{PS-SH} \leq 30\%$ (volume fraction of thiol-terminated PS in the composite), distinct peaks are seen at $Q/Q^* = 1{:}\sqrt{3}{:}\sqrt{7}$, indicating the hexagonally packed cylinder phase. With an increase in the ϕ_{PS-SH} to 40.7% and 50.7%, an additional broad peak appears at $Q/Q^* = \sim 1.30$ as well as a dramatic shift in Q of the first-order peak occurs. This broad feature is presumably caused by the combination of two peaks at $Q/Q^* = \sqrt{4/3}$ and $\sqrt{2}$, suggesting the occurrence of order−order transition from a cylindrical to a spherical structure due to the mixing of the body-centered and face-centered cubic packing. This result is consistent with the effect of incorporation of homopolymers in block copolymers.[54,56,57] From these data, we can confirm that the addition of nanoparticles reduces the degree of segregation and induces an order−disorder transition.

In the phase diagram (Figure 8a), order−order transitions are seen in PS−PVP(65) and PS−PVP(68) with $\phi_{Au} = 17.8\%$, and in PS−PVP(65) with $\phi_{Au} = 27.1\%$. Compared to the SAXS patterns of PS−PVP(65) with $\phi_{Au} = 17.8\%$ and $\phi_{Au} \sim 8.8\%$ (data not shown), additional weak peaks appear at $Q/Q^* = \sqrt{20/6}$, $\sqrt{50/6}$, $\sqrt{62/6}$, and $\sqrt{64/6}$, indicating the presence of a gyroid phase. The absence of lower order peaks is presumably due to the presence of strong broad peaks corresponding to the lamellar phase that probably smears the gyroid phase patterns. We denote the region of the phase map for PS−PVP(65) with $\phi_{Au} = 17.8\%$ as the coexisting lamellar and gyroid phases. At $\phi_{Au} = 27.1\%$, the morphology transforms to a cylindrical structure with a broad peak at $Q/Q^* = \sqrt{7}$ and a weak peak at $Q/Q^* = \sqrt{4}$.

Huh et al.[27] performed Monte Carlo simulations to predict the phase behavior of diblock copolymer/particle composites and found that the phase diagram is a function of particle size. When relatively large nanoparticles are incorporated in the minor domain ($f_{PS} < 0.5$), a new structure forms with particles in the core, surrounded by a block copolymer shell. They denote that region as the microphase-separated particles in the phase diagram. It should be noted that this phase is different from the macrophase-separated nanoparticle phase that is irregular with some nanoparticles located within the preferred domain. In the microphase-separated particle domain, the nanoparticles form condensed cylinders or lamellae within the structure of the block copolymer. Another feature in the predicted phase diagram is the coexistence regime of macrophase-separated nanoparticles and block copolymers. When the particle size decreases, the

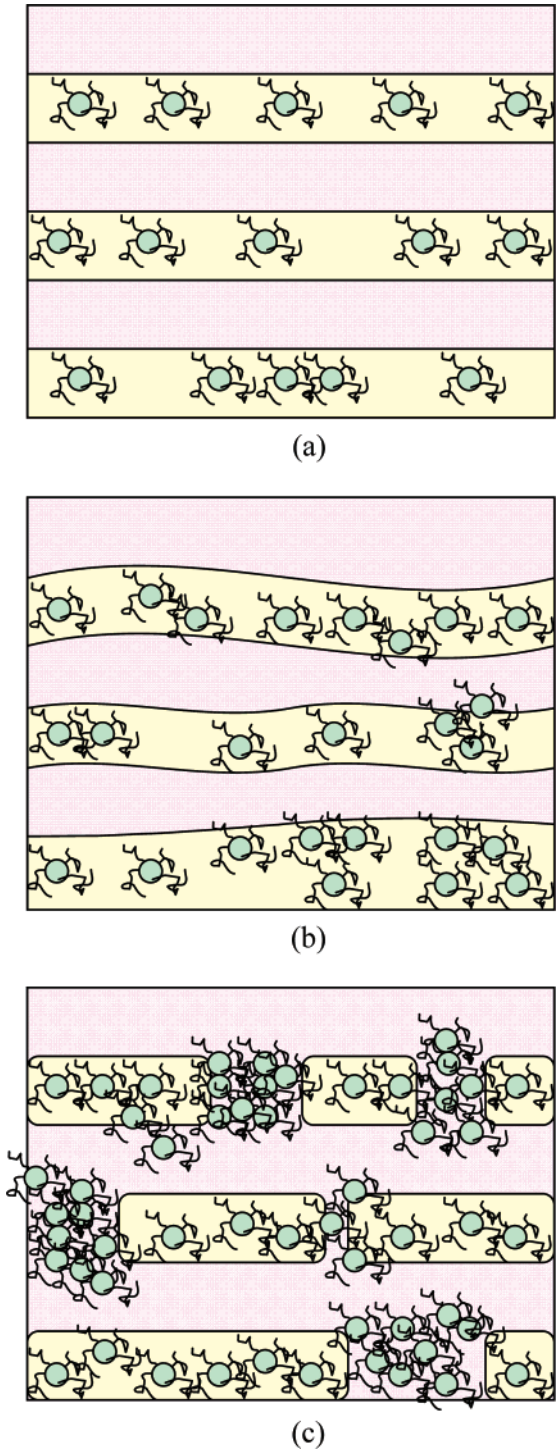

Figure 7. Schematics of the morphology of nanocomposites with the addition of nanoparticles: (a) nanoparticles well-organized in the preferred domain, (b) nanoparticles organized in the modulated domain, and (c) nanophases that have undergone macrophase separation.

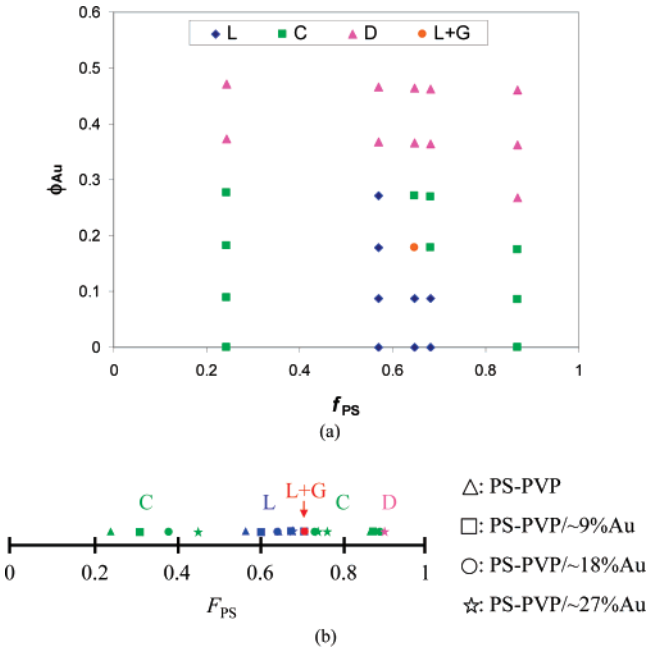

Figure 8. Phase diagram of PS−PVP/Au nanocomposites (a) as a function of f_{PS} and ϕ_{Au} and (b) as a function of the effective volume fraction, F_{PS} (L, lamellar; C, cylindrical; D, disordered; G, gyroid).

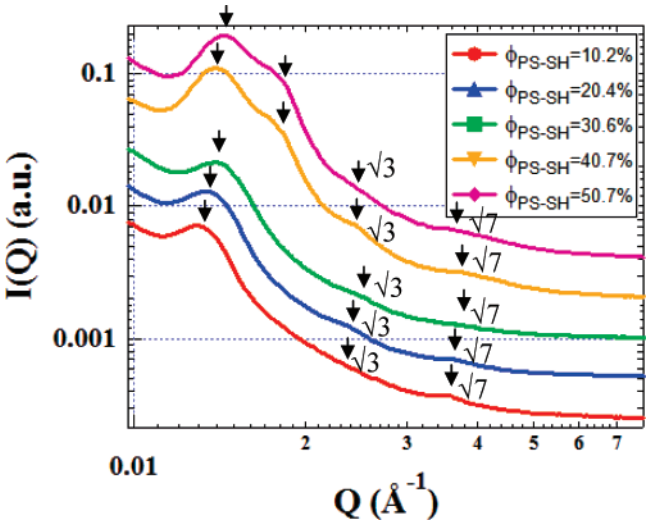

Figure 9. SAXS data of PS−PVP (f_{PS} = 0.68) with the addition of thiol-terminated PS (Scattering patterns have been shifted to increase clarity, and the arrows and numbers in the plots show the ratio of the peak positions to the value of the first-order peak).

microphase-separated nanoparticle domain disappears and the coexistence regime becomes narrower. In addition, the order−disorder transition moves toward lower particle loading due to the fact that the smaller particles are more effective in inducing an order−disorder transition. In the small particle case in this simulation, order−disorder transition occurs with increasing particle concentration regardless of f_{PS} and no microphase-separated phase was found. In our study, the degree of polymerization, N ($N = N_{PS} + N_{PVP}$) is larger than 500 (R_g > 7 nm) for all the copolymers and the particle size including the shell is 3.6 nm, which is closer to the small particle case in the simulation. In our phase diagram, we did not distinguish the two-phase region (macrophase-separated nanoparticles in the ordered block copolymers) between the ordered and disordered phases. We identify the ordered and disordered phases based on the diffraction peaks in the SAXS patterns. Except for this two-phase region, the occurrence of the order−order and order−disorder transitions in the presence of nanoparticles in our experimental phase diagram is qualitatively consistent with the simulation results in the literature.[27]

In general, the addition of nanoparticles in the preferred domain expands the domain and increases the interfacial curvature, causing an order−order transition. In our experiment, however, the increasing interfacial roughness caused by the introduction of nanoparticles negates the effect of the swelling

by the nanoparticles. Consequently, the system becomes disordered. Addition of small molecules, such as homopolymers[55] or solvents, can smooth the interface and an order−order transition can occur even at higher particle loading as shown in our studies.[37,38] We observe the occurrence of an order−order transition from cylindrical or gyroid structure even at $\phi_{Au} = 36.8\%$.

Generalized Phase Map of Bulk Nanocomposites. In the phase diagram for the bulk composites in Figure 8a, the order−order transitions depend on both f_{PS} and ϕ_{Au} for a given particle. Determination of the boundaries of the transitions involves controlling of both parameters which requires tremendous effort. Since the phase behavior of neat block copolymers as well as the block copolymers containing homopolymers is governed by the relative volume fraction of the polymers, we develop a single variable, F_{PS}, the effective PS volume fraction (volume fraction of the entire PS in the nanocomposites including the PS in PS−PVP and thiol-terminated PS associated with the Au nanoparticles) to simplify the phase diagram. The generalized phase diagram is shown in Figure 8b that allows easy determination of the phase boundaries. In Figure 8b, we only include the polymer nanocomposites with ϕ_{Au} up to ∼30% because significant macrophase separation of nanoparticles occurs at higher particle loading. At this condition, most particles do not incorporate into the PS domain which makes it difficult to estimate the F_{PS}. In Figure 8b, it can be seen that the phase behavior of PS−PVP/Au nanocomposites at low particle loading can be predicted qualitatively by using the F_{PS}. At $24.2\% < F_{PS} < 45.2\%$, a cylinder structure is observed. At $45.2\% < F_{PS} < 70.0\%$, the neat PS−PVP and its composite have a lamellar structure. With an increase in the volume fraction of the PS domain, the system undergoes an order−order transition from lamellar to gyroid. At $F_{PS} \sim 71.0\%$, the onset of a gyroid phase occurs, but a well-controlled sample processing is required to obtain a single gyroid structure. At $F_{PS} > 73.5\%$, another order−order transition from gyroid to cylinder phase occurs. This demonstration of the relationship between the phase behavior of PS−PVP/Au and the F_{PS} will be useful to predict the morphology of polymer nanocomposites.

Conclusion

The phase behavior of PS−PVP/Au nanocomposites was studied using ASAXS and TEM. The morphology of these novel nanocomposites shows strong dependence on the particle concentration and composition of PS−PVP. At low particle loading, the phase behavior of the composites can be predicted using the effective volume fraction (F_{PS}) of the entire PS content in the system including the PS grafts on the nanoparticles. With the addition of nanoparticles in the PS domain, particles expand them and change the interfacial curvature between PS and PVP, which induces order−order transitions. However, the introduction of nanoparticles in the preferred domain also increases the local fluctuations at the PS−PVP interface. This interfacial roughness competes with the change in the interfacial curvature, and breaks down the order in the system. At high particle concentration, the available volume in the PS domains saturates, and the excess particles form a particle-rich regime. This macrophase separation of nanoparticles and block copolymers leads to a disordered phase. The generalized phase map as a function of a single parameter (F_{PS}) provides as a tool to predict phase maps in different systems. We believe that the results from this study will enable comparison of the phase maps from various studies and will serve to validate the simulation studies of inorganic particle/block copolymer composites.

Acknowledgment. This work was benefited by the use of APS, IPNS, and CMT funded by DOE-BES under Contract No. DE-AC02-06CH11357.

References and Notes

(1) Sohn, B. H.; Cohen, R. E. *Chem. Mater.* **1997**, *9*, 264−269.
(2) Maldovan, M.; Urbas, A. M.; Yufa, N.; Carter, W. C.; Thomas, E. L. *Phys. Rev. B* **2002**, *65*, 165123.
(3) Bockstaller, M. R.; Thomas, E. L. *J. Phys. Chem. B* **2003**, *107*, 10017−10024.
(4) Buxton, G. A.; Lee, J. Y.; Balazs, A. C. *Macromolecules* **2003**, *36*, 9631−9637.
(5) Bockstaller, M. R.; Thomas, E. L. *Phys. Rev. Lett.* **2004**, *93*, 166106.
(6) Ciebien, J. F.; Clay, R. T.; Sohn, B. H.; Cohen, R. E. *New J. Chem.* **1998**, 685−691.
(7) Torquato, S.; Hyun, S.; Donev, A. *Phys. Rev. Lett.* **2002**, *89*, 266601.
(8) Buxton, G. A.; Balazs, A. C. *Phys. Rev. E* **2003**, *67*, 031802.
(9) Klingelhofer, S.; Heitz, W.; Greiner, A.; Oestreich, S.; Forster, S.; Antonietti, M. *J. Am. Chem. Soc.* **1997**, *119*, 10116−10120.
(10) Seregina, M. V.; Bronstein, L. M.; Platonova, O. A.; Chernyshov, D. M.; Valetsky, P. M. *Chem. Mater.* **1997**, *9*, 923−931.
(11) Templin, M.; Franck, A.; Du Chesne, A.; Leist, H.; Zhang, Y.; Ulrich, R.; Schadler, V.; Wiesner, U. *Science* **1997**, *278*, 1795−1798.
(12) Chan, V. Z.-H.; Hoffman, J.; Lee, V. Y.; Latrou, H.; Avgeropoulos, A.; Hadjichristidis, N.; Miller, R. D.; Thomas, E. L. *Science* **1999**, *286*, 1716−1719.
(13) Bockstaller, M.; Kolb, R.; Thomas, E. L. *Adv. Mater.* **2001**, *13*, 1783−1786.
(14) Thompson, R. B.; Ginzburg, V. V.; Matsen, M. W.; Balazs, A. C. *Macromolecules* **2002**, *35*, 1060−1071.
(15) Schultz, A. J.; Hall, C. K.; Genzer, J. *Macromolecules* **2005**, *38*, 3007−3016.
(16) Chan, Y. N. C.; Schrock, R. R.; Cohen, R. E. *Chem. Mater.* **1992**, *4*, 24−27.
(17) Chan, Y. N. C.; Craig, G. S. W.; Schrock, R. R.; Cohen, R. E. *Chem. Mater.* **1992**, *4*, 885−894.
(18) Sohn, B. H.; Cohen, R. E. *Acta Polym.* **1996**, *47*, 340−343.
(19) Tsutsumi, K.; Funaki, Y.; Hirokawa, Y.; Hashimoto, T. *Langmuir* **1999**, *15*, 5200−5203.
(20) Hashimoto, T.; Harada, M.; Sakamoto, N. *Macromolecules* **1999**, *32*, 6867−6870.
(21) Okumura, A.; Tsutsumi, K.; Hashimoto, T. *Polym. J.* **2000**, *32*, 520−523.
(22) Sohn, B. H.; Seo, B. H. *Chem. Mater.* **2001**, *13*, 1752−1757.
(23) Bockstaller, M. R.; Lapetnikov, Y.; Margel, S.; Thomas, E. L. *J. Am. Chem. Soc.* **2003**, *125*, 5276−5277.
(24) Sohn, B.-H.; Choi, J.-M.; Yoo, S. I.; Yun, S.-H.; Zin, W.-C.; Jung, J. C.; Kanehara, M.; Hirata, T.; Teranishi, T. *J. Am. Chem. Soc.* **2003**, *125*, 6368−6369.
(25) Lin, Y.; Boker, A.; He, J.; Sill, K.; Xiang, H.; Abetz, C.; Li, X.; Wang, J.; Emrick, T.; Long, S.; Wang, Q.; Balazs, A. *Nature (London)* **2005**, *434*, 55−59.
(26) Chiu, J. J.; Kim, B. J.; Kramer, E. J.; Pine, D. J. *J. Am. Chem. Soc.* **2005**, *127*, 5036−5037.
(27) Huh, J.; Ginzburg, V. V.; Balazs, A. C. *Macromolecules* **2000**, *33*, 8085−8096.
(28) Thompson, R. B.; Ginzburg, V. V.; Matsen, M. W.; Balazs, A. C. *Science* **2001**, *292*, 2469−2472.
(29) Lee, J.-Y.; Thompson, R. B.; Jasnow, D.; Balazs, A. C. *Phys. Rev. Lett.* **2002**, *89*, 155503.
(30) Lee, J. Y.; Thompson, R. B.; Jasnow, D.; Balazs, A. C. *Macromolecules* **2002**, *35*, 4855−4858.
(31) Lee, J. Y.; Thompson, R. B.; Jasnow, D.; Balazs, A. C. *Faraday Discuss.* **2003**, *123*, 121−131.
(32) Lee, J. Y.; Shou, Z.; Balazs, A. C. *Macromolecules* **2003**, *36*, 7730−7739.
(33) Lee, J. Y.; Shou, Z.; Balazs, A. C. *Phys. Rev. Lett.* **2003**, *91*, 136103.
(34) Chervanyov, A. I.; Balazs, A. C. *J. Chem. Phys.* **2003**, *119*, 3529−3534.
(35) Reister, E.; Fredrickson, G. H. *J. Chem. Phys.* **2005**, *123*, 214903.
(36) Bockstaller, M. R.; Mickiewicz, R. A.; Thomas, E. L. *Adv. Mater.* **2005**, *17*, 1331−1349.
(37) Lo, C.-T.; Lee, B.; Winans, R. E.; Thiyagarajan, P. *Macromolecules* **2007**, *40*, 641−647.
(38) Lo, C.-T.; Lee, B.; Winans, R. E.; Thiyagarajan, P. *Macromolecules* **2006**, *39*, 6318−6320.
(39) Ribbe, A. E.; Okumura, A.; Matsushige, K.; Hashimoto, T. *Macromolecules* **2001**, *34*, 8239−8245.
(40) Kim, B. J.; Bang, J.; Hawker, C. J.; Kramer, E. J. *Macromolecules* **2006**, *39*, 4108−4114.

(41) Kim, B. J.; Chiu, J. J.; Yi, G.-R.; Pine, D. J.; Kramer, E. J. *Adv. Mater.* **2005**, *17*, 2618−2622.
(42) Jain, A.; Gutmann, J. S.; Garcia, C. B. W.; Zhang, Y.; Tate, M. W.; Gruner, S. M.; Wiesner, U. *Macromolecules* **2002**, *35*, 4862−4865.
(43) Yeh, S.-W.; Wu, T.-L.; Wei, K.-H.; Sun, Y.-S.; Liang, K. S. *J. Polym. Sci., Polym. Phys. Ed.* **2005**, *43*, 1220−1229.
(44) Yeh, S.-W.; Wei, K.-H.; Sun, Y. S.; Jeng, U.-S.; Liang, K. S. *Macromolecules* **2005**, *38*, 6559−6565.
(45) Yeh, S.-W.; Wei, K.-H.; Sun, Y.-S.; Jeng, U.-S.; Liang, K. S. *Macromolecules* **2003**, *36*, 7903−7907.
(46) Ho, R.-M.; Lin, T.; Jhong, M.-R.; Chung, T.-M.; Ko, B.-T.; Chen, Y.-C. *Macromolecules* **2005**, *38*, 8607−8610.
(47) Yee, C. K.; Jordan, R.; Ulman, A.; White, H.; King, A.; Rafailovich, M.; Sokolov, J. *Langmuir* **1999**, *15*, 3486−3491.
(48) Lee, B.; Lo, C.-T.; Seifert, S.; Dietz Rago, N. L.; Winans, R. E.; Thiyagarajan, P. *Macromolecules* **2007**, *40*, 4235−4243.
(49) Bartlett, P.; Ottewill, R. H. *J. Chem. Phys.* **1992**, *96*, 3306.
(50) Olvera, de la Cruz, M. *J. Chem. Phys.* **1989**, *90*, 1995−2002.
(51) Whitmore, M. D.; Noolandi, J. *J. Chem. Phys.* **1990**, *93*, 2946−2955.
(52) Lodge, T. P.; Pan, C.; Jin, X.; Liu, Z.; Zhao, J.; Maurer, W. W.; Bates, F. S. *J. Polym. Sci., Polym. Phys. Ed.* **1995**, *33*, 2289−2293.
(53) Hanley, K. J.; Lodge, T. P. *J. Polym. Sci., Polym. Phys. Ed.* **1998**, *36*, 3101−3113.
(54) Winey, K. I.; Thomas, E. L.; Fetters, L. J. *Macromolecules* **1992**, *25*, 2645−2650.
(55) Hamdoun, B. *Inorg. Mater.* **2004**, *40*, 949−954.
(56) Matsen, M. W. *Macromolecules* **1995**, *28*, 5765−5773.
(57) Likhtman, A. E.; Semenov, A. N. *Macromolecules* **1997**, *30*, 7273−7278.

MA070835V